

**SCALING OF COUNTER-CURRENT IMBIBITION
PROCESSES IN LOW-PERMEABILITY
POROUS MEDIA**

SUPRI TR – 121 Report

By

A. R. Kavscek, D. Zhou, L. Jia, and J. Kamath

December 2000

Work Performed Under Contract No. DE-FC26-00BC15311

**Prepared for
U.S. Department of Energy
Assistant Secretary for Fossil Energy**

**Thomas Reid, Project Manager
National Petroleum Technology Office
P.O. Box 3628
Tulsa, OK 74101**

Table of Contents

	<u>Page</u>
List of Tables	iii
List of Figures	iii
Acknowledgements	iv
Abstract	v
1. Introduction	1
2. Experimental Study	4
2.1 Procedure	6
2.2 Results	8
3. Theoretical Analysis	10
4. Discussion	13
4.1 Scaling of Simulation Data	13
4.2 Scaling of Experimental Data	14
4.3 Counter-Current Versus Co-current Imbibition	14
5. Conclusions	16
6. Nomenclature	17
7. References	18

List of Tables

	<u>Page</u>
1. Diatomite Core Properties	20
2. Properties of Experimental Fields	20

List of Figures

	<u>Page</u>
1. Schematic of imbibition cell set up for counter current imbibition.	20
2. Porosity images of diatomite cores (left to right) used for counter current Imbibition: (1) air/water, (2) n-decane/water, (3) blandol/water, (4) n-decane/water, and (5) n-decane/water.	21
3. Nonwetting fluid recovery versus absolute time.	21
4. CT-derived water saturation images of counter current water/air imbibition in diatomite. Time is given in minutes beneath the images.	21
5. CT-derived water saturation images of counter current water/n-decane Imbibition in diatomite. Time is given in minutes given beneath the images.	22
6. CT-derived water saturation images of counter current water/blandol Imbibition in diatomite. Time is given in minutes beneath the images.	22
7. Scaling of the simulated oil recovery using the dimensionless time of Zhang <i>et al.</i> (1996): (a) logarithmic and (b) linear axes for time.	23
8. Scaling of the simulated oil recovery using the proposed dimensionless Time.	24
9. Correlation of recovery by counter current imbibition from diatomite using The proposed dimensionless time. Nonwetting-phase viscosity varies by 4 Orders of magnitude.	24

Acknowledgements

This work was prepared with the support of the U.S. Department of Energy, under Award No. DE-FC26-00BC15311. However, any opinions, findings, conclusions, or recommendations expressed herein are those of the authors and do not necessarily reflect the views of the DOE.

Additional support was provided by the Chevron Petroleum Technology Corporation and the Stanford University Petroleum Research Institute (SUPRI-A) Industrial Affiliates. These contributions are gratefully acknowledged.

Abstract

Oil recovery from low permeability reservoirs is strategically important because of the large resources locked in such formations. Imbibition is fundamental to oil recovery from such reservoirs under most secondary and improved recovery processes of practical interest. It is also characteristic of porous medium wettability. The rate and the extent of imbibition depend critically on the viscosity of the wetting and nonwetting phases. In this study, we present our recent work on imaging imbibition in low permeability porous media (diatomite) with X-ray computed tomography. The viscosity ratio between nonwetting and wetting fluids is varied over several orders of magnitude yielding different levels of imbibition performance. We also perform a mathematical analysis of counter-current imbibition processes and develop a modified scaling group incorporating the mobility ratio. This modified group is physically based and appears to improve scaling accuracy of countercurrent imbibition significantly.

1. Introduction

Petroleum production has, rightly, focused on the easiest to produce prospects. With more fields approaching maturity and abandonment, recovery options are required for more difficult to produce reservoirs such as low permeability diatomite and chalk formations. For example, estimates place the amount of original oil (OOIP) in the diatomaceous and siliceous shale formations of California at 12 to 18 billion bbl (Ilderton *et al.*, 1996). Although the volumes of oil in place are large, the low permeability creates challenging issues in producing this oil. Injectivity and productivity are generally low, and wells usually require hydraulic fracturing or in-place natural fractures to attain economic rates. Because of the limited injectivity, recovery processes must be designed carefully and natural oil-production forces optimized.

In spontaneous imbibition, wetting fluid is drawn into rock by capillary suction and the non-wetting fluid is expelled. The rate and the extent of imbibition depend critically on the viscosity of the wetting and nonwetting phases. Other factors include: fluid/fluid interfacial tension (IFT), pore structure, the initial water saturation of the rock, and relative permeability curves. Water injection, steam injection, and CO₂ injection in a water-alternating gas (WAG) fashion all rely to some extent on capillary imbibition to aid oil production. Steam injection is, for all practical purposes, carried out under saturated conditions with some fraction of the injected steam in the liquid phase. Likewise, initial heating of a cold reservoir is accompanied by condensation and flow of the resulting hot water away from the injector. In CO₂ injection under both miscible and immiscible conditions, water slugs are usually injected with the aim of controlling CO₂ mobility. Thus, capillary phenomena are important to most recovery techniques of interest in low permeability media.

Imbibition can occur in a reservoir in both counter-current and co-current flow modes, depending on the fracture network and the water injection rates. Bourblaux and Kalaydjian (1990) studied co-current and countercurrent imbibition in natural sandstone samples. They reported significantly lower imbibition rates from counter-current experiments as compared to co-current experiments. They suggested that low counter-current imbibition rates are due to flow patterns and the extra viscous resistance generated when the two phases pass each other. They also

observed some difference in final oil recovery from the two processes. Note that Bourblaux and Kalaydjian (1990) use a single mineral oil (Soltrol 130, $\mu_{nw}=1.5$ mPa-s) as the nonwetting phase in their experiments. They did not consider how different oil viscosities might change the imbibition rate and final oil recovery.

Empirical scaling models have been proposed to estimate oil recovery rates from blocks that have sizes and shapes different from laboratory core samples (*e.g.*, Morrow *et al.* 1994, Zhang *et al.* 1996, Zhou *et al.* 2000). Kazemi *et al.* (1992) presented numerical and analytical solutions of oil recovery using empirical, exponential transfer functions based on the experimental data given by Aronofsky *et al.* (1958) and Mattax and Kyte (1962). They proposed a shape factor that included the effect of size, shape, and boundary conditions of the matrix. More recently, this shape factor was generalized by Zhang *et al.* (1996) to account for sample shape and boundary conditions more accurately. A dimensionless time, t_D , was proposed that reads

$$t_D = t \sqrt{\frac{k}{\phi} \frac{\sigma}{\mu_s L_c^2}} \quad (1)$$

where k is absolute permeability and σ is interfacial tension. The characteristic length, L_c , is a function of the bulk volume of the rock sample and the area of the block face open to imbibition. The geometric average of phase viscosity, μ_s , is given by the following equation:

$$\mu_s = \sqrt{\mu_w \mu_{nw}} \quad (2)$$

The above scaling equation was used by Zhang *et al.* (1996) and they report that ultimate oil recovery on a pore volume basis by spontaneous imbibition in Berea sandstone cores is approximately constant for systems with differing lengths, viscosity ratios, and boundary conditions. Zhang *et al.* (1996) emphasize that the use of the square root of viscosities in correlation of imbibition is empirical and that air/liquid results did not correlate with those for oil/water systems.

Whereas imbibition has long been recognized as an important recovery mechanism in low permeability reservoirs, most studies were performed on sandstone cores with relatively high

permeability (>100 mD) (e.g., Jadhunandan and Morrow 1991, Reis and Cil 1993, Cil and Reis 1996, Garg *et al.*, 1996). Both chalk and diatomite formations have high porosity (35 to 70%) and low permeability (0.1 to 10 mD). Diatomite is a siliceous rock composed mainly of biogenic silica and detrital-rich layers of sand, silt and clay; whereas, chalk is a carbonate. Notable work regarding chalk rock systems includes Cueic *et al.* (1994) who found experimentally that oil recovery by water imbibition is rapid and efficient for strongly water-wetting chalk. Reduction in IFT decreased the rate of imbibition but increased ultimate oil recovery. This effect was attributed to the mobilization of oil ganglia. Milner and Øxnevad (1996) evaluated imbibition recovery of different chalk facies and linked performance to the rock framework and pore system. In regard to diatomite, Akin *et al.* (2000) report the use of a novel X-ray computed tomography (CT) imbibition cell to quantify co-current imbibition rates and saturation profiles as well as to begin linking diatomite imbibition performance to pore structure and roughness. Kamath *et al.* (1995), conducted long-term forced displacements on diatomaceous mudstone samples revealing that water-oil relative permeability end points could be sensitive to flooding velocity. Relative permeability to water increased by as much as 31% with increased flow rate.

Low permeability rocks, such as diatomite, are relatively unstudied in the laboratory because of low injectivity and a host of other difficulties in designing and performing laboratory tests on such samples. The low rates and long turn over time are major contributors to measurement uncertainties. For example, we observed substantial differences in residual oil saturation in diatomite between counter-current imbibition and co-current imbibition. The high residual oil saturation from free imbibition may be due to insufficient imbibition time, or due to the difference in flow patterns. A good understanding of the flow characteristics of the imbibition process and its scaling would be helpful for interpretation.

In this paper, we report an experimental and scaling study of counter-current imbibition in diatomite. Despite some similarities between chalk and diatomite, generalization of imbibition performance between these two rock types is not currently possible. Our aim is to collect in-situ water saturation profiles and imbibition performance data across several orders of magnitude of the ratio of wetting to nonwetting fluid viscosity. Within this paper, much of the experimental

focus is placed on counter-current imbibition to complement previous work on co-current imbibition (Akin *et al.* 2000). We also propose a one-dimensional model to analyze the scaling behavior of counter-current imbibition processes.

2. Experimental Study

Our objectives are to obtain the saturation profile and rate of imbibition in order to determine fluid displacement mechanisms during counter-current water imbibition into air- and oil-filled cores. We use X-ray CT scanning for in-situ visualization of displacement patterns. Our porous medium is a well characterized diatomite outcrop sample.

An imbibition cell designed specifically for the CT scanner is used. Both counter-current and co-current imbibition are possible with the setup. The scan geometry is unique. In conventional CT-scanning many scans closely spaced in time are required to determine accurately the position and shape of displacement fronts. Rather than scan in a conventional mode where X-ray CT data is collected in cylindrical volume sections that are normal to the central axis of the core, the entire length of the core is scanned at the same instant as illustrated in Figure 1. Because we scan along the direction of flow, a single slice provides us with a picture of the progress and saturation pattern of imbibition. Nonlinearity in flow behavior and the effect of heterogeneities are thereby easily gauged. This change in scan orientation required redesigning the coreholder assembly such that beam hardening and x-shaped imaging artifacts caused by asymmetry in the shape of the scanning plane are minimized. Figure 1 details this special design. There are two separate chambers fashioned from acrylic tubes. The main chamber is the core holder and the second is a water jacket of circular cross section that surrounds the core. Cores are potted inside the acrylic tube with epoxy (Epoxy 907, Miller-Stephenson Chemical Co.). There is no fluid exchange between the two chambers and the outer water-filled chamber allows for some measure of temperature control. The core holder may be placed in either a horizontal or vertical position. For this work, vertical is chosen. An L-shaped mounting bracket allows for bolting of the apparatus to a precision positioning system (Compumotor RP240, Parker-Hannifin Corp).

Images obtained with this setup are flat and do not exhibit detectable positioning errors. Further details are given by Akin *et al.* (2000).

The core holder has two endcaps, shown schematically at the top and bottom of the core, for fluids to flow in and out of the core holder. Specifics of the endcaps depend upon whether co-current or counter-current imbibition is studied. For counter-current experiments, an endcap that allows water to be circulated by pump across the core face is used. The endcap contains a fracture-like gap of 5 mm and inlet/outlet flow lines. Thus, a supply of fresh water is maintained at the core face and produced oil is swept out of the endcap. For co-current experiments, endcaps with spider-web shaped channels are used to distribute the flow evenly.

Our CT-scanner is a Picker 1200 SX X-ray scanner with 1200 fixed detectors. The voxel dimension is (0.5 mm by 0.5 mm by 10 mm), the tube current is 50 mA, and the energy level of the radiation is 140 keV. The porosity and aqueous-phase saturation fields are measured on a single vertical volume section in the center of the core as a function of time. The acquisition time of one image is 3 seconds while the processing time is around 40 seconds. The total time of measurement is short enough to capture accurately the position of the front and construct the saturation profiles along the core.

Diatomite samples were obtained from the Grefco Quarry (Lompoc, CA). They had no initial oil or water saturation. The rock is consolidated and almost pure white indicating little silt or mud. Some evidence of bedding planes is visible to the naked eye. The samples are from outcrop or near surface formations; hence, silica is in the amorphous or opal-A state. Previous work with this type of diatomite has demonstrated that the rock is water wet, pore structure is complex, and flow pathways are well connected (Akin *et al.* 2000). The rock is cut in a direction parallel to the bedding plane and shaped into cylindrical cores with diameters of 2.5 cm and lengths of 9.5 cm. The diatomite block could not be cored using conventional drilling and cutting methods because of its friable nature. A piece of the rock is cut by band saw to approximate dimensions. Then it is shaped manually by fixing two circular 1 inch patterns to each end of the rough-cut core. These pieces are used as guides in the shaping process with a file. Final shaping is

achieved with sandpaper. Nominal porosity and permeability values are 72% and 6 mD as summarized in Table 1.

2.1 Procedure

The experimental procedure depends slightly upon whether water/air or water/oil imbibition is performed. The core is exposed to house vacuum and a temperature of 50 °C for a minimum of ten hours and usually several days, to ensure a "dry" core at the beginning of the experiment. The end caps are placed on the core holder and the core holder is placed inside the water jacket vertically and leveled. Since the core holder is surrounded by water during the CT experiments, a leak test is performed by applying a slight gas pressure and checking that the pressure in the core holder is maintained for a period of time. The water jacket is then filled with water and a dry image of the core is taken to obtain the reference dry core CT values.

In all cases, we begin imbibition with the core completely filled with nonwetting fluid (air or oil). This avoids the added complication to interpretation introduced by variable initial water saturation and allows direct comparison to the water-air case. With this well characterized and easily repeatable initial condition we hope to show definitively the effect of viscosity ratio on imbibition performance of diatomite.

2.1.1 Water-Air Experiments

For water-air experiments, water is introduced at the top of the core. Water is supplied by a reciprocating chromatographic pump (Constametric 3200, LDC Analytical) and pumped through the endcap at a rate of 5 cm³/min. Pressure drop across the endcap is below 100 Pa because flow spaces within the endcap have large dimensions. Thus, ample water is supplied at the core face and imbibition is spontaneous rather than forced. The outlet endcap at the bottom of the core is sealed shut ensuring that imbibition is counter current.

Once imbibition begins, CT images are taken periodically. Initially, images are taken at roughly 1 min intervals and the frequency of scanning decreases as the rate of imbibition slows.

Image collection ceases when CT numbers stabilize. De-aerated water is pumped through the core after imbibition to ensure that the core is completely filled with water.

Saturation profiles during imbibition are constructed from raw CT data according to

$$S_w = \frac{CT_{ob} - CT_{ar}}{CT_{wr} - CT_{ar}} \quad (3)$$

where CT denotes the CT value for a voxel and the subscripts ob, ar, and wr refer to the object being processed, air-saturated rock, and water-saturated rock, respectively.

Because images of 100% air and water filled rock are available, a map of porosity for each core can be computed from

$$\phi = \frac{CT_{wr} - CT_{ar}}{CT_w - CT_a} \quad (4)$$

The subscript w refers to the CT number of the water phase whereas a refers to air. Water and air CT numbers are taken as 0 and -1000, respectively. Figure 2 presents porosity images of the cores used in these experiments. Black shading corresponds to a porosity of 0.6 while white is 0.8. Note that the last core exhibits some diagonally oriented planes of high porosity.

2.1.2 Water-Oil Experiments

Cores are dried as described above. Then oil is introduced to the core through the bottom end cap (Fig. 1) with the top end cap open to atmosphere. Thus, the core is saturated in a co-current fashion. Oil is pumped through the core to dissolve any residual air. At this stage, the lower inlet to the core is sealed shut. The porosity field of cores used for oil-water imbibition are calculated using Eq. (4) upon substitution of CT_o , the CT number for the oil phase, for CT_w and replacing CT_{wr} with CT_{or} , the CT number of the oil saturated rock.

For counter-current imbibition, water is again introduced at the top of the core by pumping water through the endcap at a rate of 5 cm³/min. Water that did not imbibe and any produced oil exit the end cap. Images are collected periodically throughout the duration of

imbibition. It is very difficult to obtain a 100% water-saturated image within the same experiment and a slightly different equation is used to process the raw CT data:

$$S_w = \frac{CT_{ob} - CT_{or}}{\phi(CT_w - CT_o)} \quad (5)$$

where ϕ is the independently measured porosity of each voxel. Equation (5) is comparable with Eq. (3) in terms of accuracy because images obtained here are flat and exhibit minimal artifacts or errors.

Two oils with different viscosities are used. The first is n-decane whose viscosity is 0.84 mPa-s whereas the second is a viscous white mineral oil (Blandol) whose viscosity is 25.2 mPa-s. The effect of using these different oils is solely to adjust the oil-water viscosity ratio. Even though cores are oriented vertically, buoyancy forces within the cores are negligible relative to capillary forces. The Bond number ($=(\rho_w - \rho_o)gk/\sigma$) for water-oil cases is approximately 10^{-10} and 10^{-9} for water-air cases indicating the dominance of capillarity. The relevant properties of the experimental fluids are summarized in Table 2. The Blandol was passed through a column of activated carbon before measurement to remove any surface active impurities. This process increased the Blandol-water interfacial tension by roughly 3 mN/m.

2.2 Results

Our chief point of interest from the experiments is counter-current imbibition performance as the ratio of nonwetting fluid to wetting fluid viscosity increases. Figure 3 summarizes the recovery versus time for all experiments. Recovery is normalized by the total volume of nonwetting fluid originally present in the core. Three water/n-decane experiments were conducted to assure repeatability. However, the cores all have different permeability and so water/n-decane results do not fall onto a single curve. As expected, imbibition recovery slows as non-wetting fluid viscosity and flow resistance increases. Nevertheless, imbibition is relatively

rapid in all cases due to strong capillary forces despite the low rock permeability. Residual oil saturations are reported in Table 1.

The saturation images obtained from the raw CT data illustrate the strong capillary forces that are operative during imbibition. In all of the images to be discussed, black indicates that S_w is 0 while white indicates that S_w is 1. Figure 4 presents results from air-water imbibition at various points in time. Water enters the core from the top and movement down the core is roughly one-dimensional. The water front is relatively sharp initially and becomes more diffuse as the front moves through the core. Front movement is rapid and it reaches the end of the core at 180 min. By comparing Fig. 4 with Fig. 9 of Akin et al (2000) which presents water-air co-current imbibition results for the same rock, we find that counter-current imbibition is relatively slower and that the imbibition fronts are more diffuse.

Figure 5 shows saturation images from n-decane water imbibition and Figure 6 gives results for the blandol water system. Note the shaded bar in each figure indicating S_w . As the oil viscosity increases by a factor of roughly 20 between Figs. 4 and 5, imbibition displacement effectiveness decreases. Figure 6 lacks a discernable displacement front while such a feature is evident in Fig. 5. When the imbibition front reaches the end of the core, recovery in the n-decane case is roughly 0.65 whereas at the higher viscosity recovery is about 0.5. As the nonwetting phase viscosity and fluid flow resistance increases, it becomes increasingly hard for the oil to move in a countercurrent fashion across the region of high water saturation at the inlet of the cores.

There are several aspects of Figs. 5 and 6 that deserve further comment. We note that counter-current imbibition, while generally occurring in a one-dimensional fashion, is sensitive to local inhomogeneities within the rock. In Fig. 5 the displacement front becomes somewhat tilted because the capillary characteristics of the rock are not constant. Compare images at times of 27 min and 158 min within Fig. 5. Careful observation of the images in Fig. 6 reveals that water begins to accumulate near the bottom of the core at roughly 77 min. This is well before the macroscopic front arrives. Apparently some rapid conduit with high permeability allowed water to move down the core rapidly. Indeed, this core exhibits high porosity regions roughly diagonal

to the axis of the core, see Fig. 2. Previous work examining co-current imbibition in this same rock found that imbibition frontal advance was nearly one-dimensional (Akin et al 2000).

To summarize the experimental results, imbibition performance as gauged by speed of oil recovery and amount recovered decreases as the non-wetting phase viscosity increases. Water movement through the cores becomes increasingly diffuse with viscosity.

3. Theoretical Analysis

In this section, we derive imbibition rates by assuming that flow is one dimensional and the fluids are incompressible. Also, assumed is that the wettability and pore structure of the system are similar across the medium. We neglect any effect of gravity. Applying Darcy's law and invoking capillarity results in the following equations:

$$u_w = \frac{-kk_{rw}}{\mu_w} \frac{\partial p_w}{\partial x} = -\lambda_w \frac{\partial p_w}{\partial x} \quad (6)$$

$$u_{nw} = \frac{-kk_{rnw}}{\mu_{nw}} \frac{\partial p_{nw}}{\partial x} = -\lambda_{nw} \frac{\partial p_{nw}}{\partial x} \quad (7)$$

$$u_t = u_{nw} + u_w \quad (8)$$

$$P_c = P_{nw} - P_w \quad (9)$$

where u is Darcy velocity, k is absolute permeability, k_r is relative permeability, μ is viscosity, p is pressure, and λ is mobility. The subscripts nw , w , c , and t represent nonwetting phase, wetting phase, capillary, and total, respectively. Upon combination and rearrangement of Eqs. (6) to (9), we obtain for the wetting phase pressure gradient

$$\frac{\partial p_w}{\partial x} = \frac{-u_t}{\lambda_t} - f_{nw} \frac{\partial p_c}{\partial x} \quad (10)$$

where f represents fractional flow ($=\lambda_{nw}/\lambda_t$) and λ_t ($=\lambda_{nw}+\lambda_w$) is the total mobility.

Consider now the case of counter-current imbibition. The total velocity must be 0 at all points within the one-dimensional media because the fluids are assumed to be incompressible. Setting u_t within Eq. (10) to 0 and back substituting into Eq. (6) results in

$$u_w = \frac{\lambda_w \lambda_{nw}}{\lambda_t} \frac{\partial p_c}{\partial x} \quad (11)$$

Note that Eq. (11) does not neglect the pressure gradient within the wetting phase. The form of Eq. (11) results from the restriction to counter-current flow and it suggests correctly that the imbibition rate depends upon individual phase mobilities and the total mobility of the system.

To proceed, Eq. (11) is multiplied and divided by $\sqrt{k_{rw} k_{rnw} / \mu_w \mu_{nw}}$. This operation and some rearrangement yields

$$u_w = k \frac{1}{\sqrt{\mu_w \mu_{nw}}} \frac{\sqrt{k_{rnw} k_{rw}}}{\sqrt{M} + \frac{1}{\sqrt{M}}} \frac{\partial P_c}{\partial S_w} \frac{\partial S_w}{\partial x} \quad (12)$$

where $M (= (\mu_{nw} k_{rw} / \mu_w k_{rnw}))$ is the mobility ratio.

The form of Eqs. (11) and. (12) results from the restriction to counter-current flow. It suggests that counter-current imbibition is diffusion-like and controlled by the product of the mobility in both phases. Note that in Eq. (12), the effects of viscosity are accounted for by $\sqrt{\mu_{nw} \mu_w}$ and $\sqrt{M} + \frac{1}{\sqrt{M}}$. The values of the second term are not very sensitive to M , when M is not significantly larger or smaller than unity. However, when the value of M is substantially different from unity, the contribution of $\sqrt{M} + \frac{1}{\sqrt{M}}$ can be significant. The following dimensionless time follows from Eq. (12)

$$t_D = t \sqrt{\frac{k}{\phi}} \frac{\sigma}{L_c^2} \sqrt{\lambda_{rw}^* \lambda_{rnw}^*} \frac{1}{\sqrt{M^*} + \frac{1}{\sqrt{M^*}}} \quad (13)$$

where $\lambda_r^* (= k_r^* / \mu)$ is a characteristic mobility for the wetting and nonwetting phases and M^* ($= \lambda_{rw}^* / \lambda_{rnw}^*$) is a characteristic mobility ratio. Here, end-point relative permeabilities are used when calculating λ_r^* and M^* . Equation (13) is similar to the empirically determined (Zhang et al 1996) scaling of t_D indicated in Eqs. (1) and (2) with respect to phase viscosity. In the limit of M^* approaching unity, t_D varies inversely with the geometric mean of μ_{nw} and μ_w . Note also that Eq. (13) explains water/gas imbibition scaling. For water/gas cases, $\sqrt{M^*} \ll 1 / \sqrt{M^*}$ and the scaling of t_D with viscosity is approximately $1/\mu_w$ as indicated empirically (*c.f.*, Handy 1960).

The mobility ratio depends on the viscosity of the fluids and the wettability of the system. For strongly water-wet systems, the end-point relative permeability of the wetting phase can be significantly less than unity (Dullien 1992). For water-wet sandstone, water relative permeability can be as low as 0.05 at residual oil saturation. Therefore, the mobility ratio can be close to unity even for systems of high viscosity ratio. The diatomite samples used here are strongly water wet and their endpoint relative permeabilities are expected to be low as in the sandstone case.

The above discussion is based on the assumption that the relative permeability and the capillary pressure functions are similar for all of the measurements. In counter-current imbibition, the total water imbibed is controlled by matrix adjacent to the fracture. Thus, if S_w at the inlet does not vary significantly, the oil recovery is proportional to $\sqrt{t_D}$ until the imbibition front reaches the outlet boundary. Because values of $\partial P_c / \partial S_w$ increase as water saturation decreases, the imbibition rate is larger at low water saturation than at high water saturation. Therefore, the oil recovery may depart from $\sqrt{t_D}$ (see discussion).

To recap, the oil recovery from counter-current imbibition is approximately proportional to the square-root time during the initial infinite-acting period. The dimensionless time for counter-current imbibition can be scaled by Eq. (13), which is more general and explains the empirical findings of Zhang *et al.* (1996).

4. Discussion

Because of the complex nature of experiments associated with low permeability samples and CT scanning, only a limited number can be performed in a reasonable period of time. Additionally, we performed a number of numerical simulations of counter-current imbibition to strengthen our scaling arguments above. The capillary pressure and relative permeability curves reported for sandstone by Bourblaux and Kalaydjian (1990) were used. A two-dimensional permeability field was generated with correlation lengths of 0.05 in both directions and medium permeability of 1.0 mD. The model (100 X 100 cells) has the dimensions of 25 cm (10 in.) in length and 10 cm (4 in.) in width to mimic experiments on a whole core. Wetting liquid viscosity was kept constant (0.75 mPa-s) and nonwetting phase viscosity varied from 1.0, 20 to 200 mPa-s. The end-point mobility ratios are about 0.1, 1.9 and 19.2.

4.1 Scaling of Simulation Data

Previous scaling studies of spontaneous imbibition have focused on the shape factor proposed by Zhang *et al.* (1996) and the results are usually presented on a logarithmic time scale. The scaled recovery curves generally cover about two orders of magnitude. The large time scale can mask the differences between scaled data. In Figure 7(a), we present the simulated oil recoveries from counter-current imbibition using the dimensionless time of Zhang *et al.* The curves indeed fall into a narrow range. However, the same data are shown in Figure 7(b) with a linear time scale. An almost 100% error is indicated between the low and high viscosity oil. For low permeability reservoirs this time error might be as long as the field life. Figure 8 shows the same data scaled by the new dimensionless time with the appropriate end-point mobility ratio. Here, the endpoint relative permeabilities for the wetting and nonwetting phase are 0.05 and 0.65, respectively, consonant with the data of Bourblaux and Kalaydjian (1990). The scaling is almost perfect with slight differences at late times. These differences result from the influence of the boundary of the porous medium on imbibition.

4.2 Scaling of Experimental Data

In the simulations, the relative permeability functions and the fluid properties are known; therefore, the end-point mobility ratio is defined exactly. For the experiments, relative permeability functions are not known accurately. Nevertheless, the scaling group for time developed in §3 was tested on the available counter-current imbibition data for diatomite. For the water/air experiments, k_{rw}^* is set to 0.14 and k_{rnw}^* is chosen as 0.60. In the water/oil cases, k_{rw}^* and k_{rnw}^* are set to 0.14 and 0.45, respectively. These endpoint values are representative of fine-grained, strongly water-wet diatomite (Schembre and Kovscek 2000). Figure 9 displays the result of this exercise. Note that recovery has been scaled to the fraction of recoverable oil. The recovery from the water/air system and all of the water/oil systems agree reasonably well. Within experimental scatter, the data are reduced to a single curve in spite of the fact that the nonwetting fluid viscosity varies by 4 orders of magnitude. Both the simulation and the experimental data indicate the new dimensionless time can improve significantly the scaling of spontaneous imbibition in low permeability porous media.

The good scaling of recovery from systems with different viscosity ratios suggests that the general shapes of the recovery curves as a function of dimensionless time are similar over the viscosity range studied in this paper. The scaling of the simulation results demonstrate that the end-point mobility ratio contributes to imbibition rate significantly. The end-point mobility ratio is also a measure of the wettability of the systems. For strongly water wet rocks, such as clean sandstone, the relative permeability to water can be very small, resulting in small end-point mobility ratios. On the other hand, for weakly water-wet systems, the water-end point relative permeability can be large, resulting in large end-point mobility ratios. One needs to know the system wettability before scaling laboratory data to the field situation.

4.3 Counter-Current Versus Co-current Imbibition

In designing an oil recovery process from low permeability formations, we need to optimize the natural recovery potentials. Do we encourage counter-current or co-current

imbibition in waterflooding a reservoir? Which gives faster recovery? And which recovers more oil?

In simulating both counter-current and co-current imbibition, we used the same relative permeability and capillary pressure curves. Results from co-current imbibition, not shown here, consistently indicated about 20% more oil recovery compared to countercurrent imbibition. We carefully examined the simulated residual oil saturation distributions and found that countercurrent imbibition is much more sensitive to local heterogeneity and traps more oil as a result. Experiments and simulations indicate that co-current imbibition reaches residual oil saturation much faster than counter-current imbibition, as others have shown (*e.g.*, Bourblaux and Kalaydjian 1990). Thus, strictly applying measured residual oil saturation from counter-current imbibition experiments to the field can be pessimistic, because some degree of co-current flow might exist in the field. Nevertheless, counter-current imbibition may be the preferable recovery mechanism in low permeability reservoirs with relatively viscous oil. Oil recovery from counter-current imbibition is proportional the square-root of time. For dimensionless times less than 1, it is then expected that counter-current imbibition recovers oil faster than processes that are proportional to time. As oil viscosity increases, this period of time increases in an absolute sense as indicated in Eq. (13).

For low permeability reservoirs such as diatomite, the permeability is about 1 mD and the oil viscosity is about 10 to 20 cp. Experience has shown that pressure gradients of more than 4500 kPa/m (200psi/ft) are needed for conducting laboratory forced displacement experiments (Kamath *et al.* 1995). The reservoir pressure gradient cannot be more than 110 kPa/m (5 psi/ft), in practice, considering reservoir depth and injectivity. Clearly, oil recovery in a displacement fashion is very difficult. However, extensive fracturing of the formation and encouraging counter-current imbibition may improve access to the reservoir and promote increased field-wide recovery.

5. Conclusions

This paper reports experimental measurements of countercurrent imbibition in diatomite using novel CT imaging techniques. Imaging with X-ray CT permits quantitative monitoring of the advance of wetting liquids. Experiments were conducted with wetting and nonwetting fluids whose viscosities spanned 4 orders of magnitude. The advance of wetting liquid slows and saturation patterns become increasingly diffuse as the ratio of nonwetting to wetting liquid viscosity increases. Counter-current imbibition appears to be much more sensitive to core-scale heterogeneities as compared to co-current results in the same rock type reported elsewhere (Akin *et al.* 2000).

A theoretical analysis of the flow characteristics of imbibition processes was also conducted. A new formulation for the dimensionless time appropriate to counter-current imbibition resulted. The new scaling was used to correlate experimental and simulation results. It improves correlation significantly by taking end-point fluid-phase mobilities and the mobility ratio into account. The scaling also explains the empirical observation that water/oil imbibition time scales inversely with the geometric mean of water and oil viscosity, whereas water/air imbibition scales inversely with water viscosity.

Application of laboratory-based residual oil saturation measurements from counter-current imbibition tests to the field can lead to pessimistic predictions. This is true especially for low permeability rocks containing relatively viscous oil. While this work helps to clarify the role of mobility ratio, other factors such as rock type, wettability, and initial saturation are not well understood. In low permeability systems, t_D can be less than 1 for a portion of the total recovery time. Because, counter-current imbibition initially scales as $\sqrt{t_D}$, it recovers oil faster than processes that scale linearly with time provided that t_D is less than 1.

6. Nomenclature

CT	CT number
k	permeability
k_r	relative permeability
L_c	characteristic length
M	mobility ratio
P_c	capillary pressure
S_w	water saturation
t	time
u	Darcy velocity
ϕ	porosity
λ	mobility
ρ	mass density
σ	surface tension
μ	phase viscosity

Subscripts

a	air phase
ar	CT value of air-saturated rock
D	dimensionless
nw	nonwetting phase
o	oil phase
ob	CT value of image being processes
or	CT value of oil saturated rock
s	denotes geometric mean of phase viscosity
t	total
w	wetting phase
wr	CT value of water-saturated rock

7. References

1. Akin, S, Schembre, J. S., Bhat, S. K., and Kovsky, A. R., 2000. "Spontaneous Imbibition Characteristics of Diatomite," J. Pet. Sci. & Eng. **25**:149-165.
2. Cil, M. and Reis, J. C., 1996. "A Multi-Dimensional, Analytical Model for Counter-Current Water Imbibition into Gas-Saturated Matrix Blocks," J. Pet. Sci & Eng., **16**: 61-69.
3. Cuiec, L., Bourbiaux, J. B. and Kalaydjian, F. J., Sep 1994. "Oil Recovery by Imbibition in Low Permeability Chalk." Soc. Pet. Eng. Form. Eval. **9**: 200-208.
4. Dullien, F. A. L., 1992. Porous Media Fluid Transport and Pore Structure, 2nd Ed. Academic Press Inc, San Diego, CA.
5. Garg, A., Zwahlen, E. and Patzek, T. W., 1996. "Experimental and Numerical Studies of One-Dimensional Imbibition in Berea Sandstone". presented at the 16th Annual American Geophysical Union Hydrology Days, Fort Collins, CO, 15-18 Apr.
6. Ilderton, D. C., Patzek, T. W., Rector, J. W. and Vinegar, H. J., Mar 1996. "Passive Imaging of Hydrofractures in the South Belridge Diatomite." Soc. Pet. Eng. Form. Eval. **11**: 46-54.
7. Jadhunandan, P. P. and Morrow, N. R., 1991. "Spontaneous Imbibition of Water by CrudeOil/Brine/Rock Systems." In Situ **15**(4): 319-345.
8. Kamath, J., deZabala, E.F., and Boyer, R. E., 1995. "Water/Oil Relative Permeability Endpoints of Intermediate-Wet, Low-Permeability Rocks," Mar. 1995, Soc. Pet. Eng. Form. Eval. **10**: 4-10.
9. Kazemi, H., Gilman, J. R. and El-Sharkaway, A. M., May 1992. "Analytical and Numerical Solution of Oil Recovery from Fractured Reservoirs Using Empirical Transfer Functions". Soc. Pet. Eng. Res. Eng. **7**(2): 219-227.
10. Mattax, C. C. and Kyte, J. R., Jun 1962. "Imbibition Oil Recovery from Fractured Water-Drive Reservoirs." Soc. Pet. Eng. J. **2**: 177-184.
11. Milner, J. and Øxnevad, R. I., 1996. "Spontaneous Imbibition in Two Different Chalk Facies." Petroleum Geoscience **2**: 231-240.

12. Morrow, N. R., Ma, S., Zhou, X. and Zhang, X., 1994. "Characterization of Wettability from Spontaneous Imbibition Measurements". CIM 94-475, presented at the 45th Ann. Tech. Meeting of the Pet. Soc. of the CIM, Calgary, Alberta Canada, 12-15 Jun.
13. Reis, J. C. and Cil, M., 1993. "A Model for Oil Expulsion by Counter-Current Water Imbibition in Rocks: One-Dimensional Geometry," J. Pet. Sci & Eng., **10**: 97-107.
14. Schembre, J. M. and Kavscek, A. R. 2000. Unpublished results.
15. Zhang, X., Morrow, N. R. and Ma, S., Nov 1996. "Experimental Verification of a Modified Scaling Group for Spontaneous Imbibition." Soc. Pet. Eng. Res. Eng. **11**: 280-285.
16. Zhou, X., Morrow, N. R., and Ma, S., 2000. "Interrelationship of Wettability, Initial Water Saturation, Aging Time, and Oil Recovery by Spontaneous Imbibition and Waterflood." Soc. Pet. Eng. J. **5**: 119-207.

Table 1. Diatomite Core Properties

Core	Experimental condition	average permeability, mD (10^{-15} m^2)	average porosity, fraction	residual saturation, S_{nwr}
1	air/water	6.0	0.64	0.05
2	n-decane/water	6.1	0.72	0.30
3	blandol/water	7.9	0.77	0.34
4	n-decane/water	2.5	0.78	0.38
5	n-decane/water	4.3	0.68	0.36

Table 2. Properties of Experimental Fluids

	ρ (kg/m^3)	μ (mPa-s)	σ liquid-air (mN/m)	σ liquid-water (mN/m)	CT (H)
air (STP)	1.82	0.018	-	72	-1000
n-decane	730	0.84	23.7	51.4	-283
blandol	780	25.	20.1	45.7	-212
water	1000	1.0	72	-	0

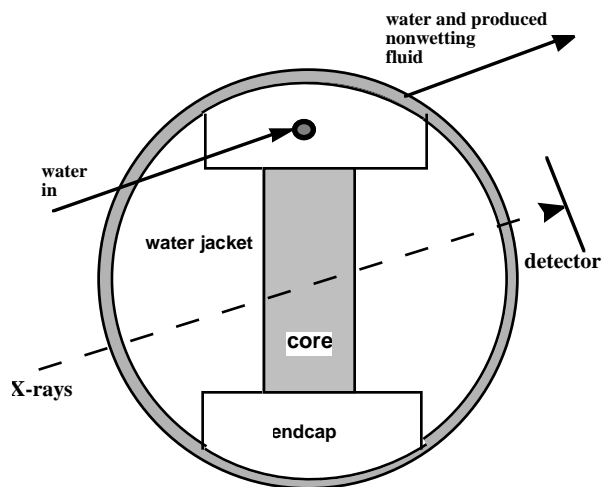


Figure 1. Schematic of imbibition cell set up for countercurrent imbibition.

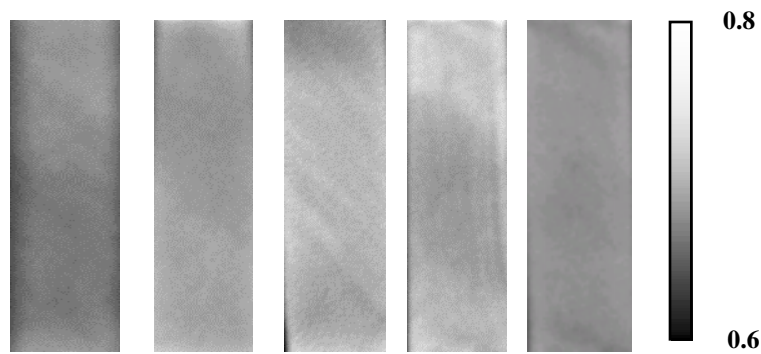


Figure 2. Porosity images of diatomite cores (left to right) used for countercurrent imbibition: (1) air/water, (2) n-decane/water, (3) blandol/water, (4) n-decane/water, and (5) n-decane/water.

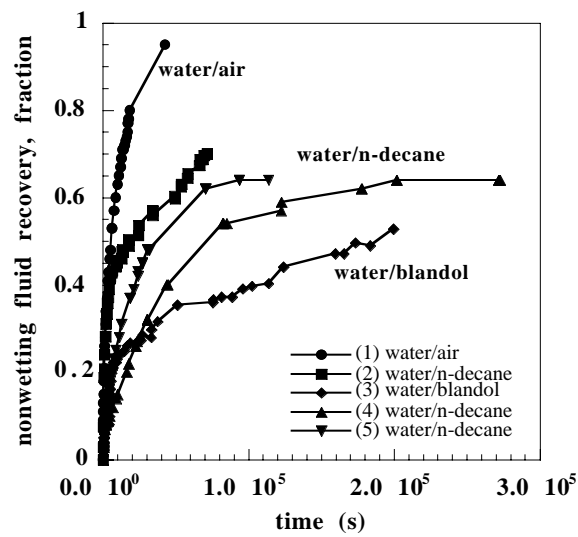


Figure 3. Nonwetting fluid recovery versus absolute time.

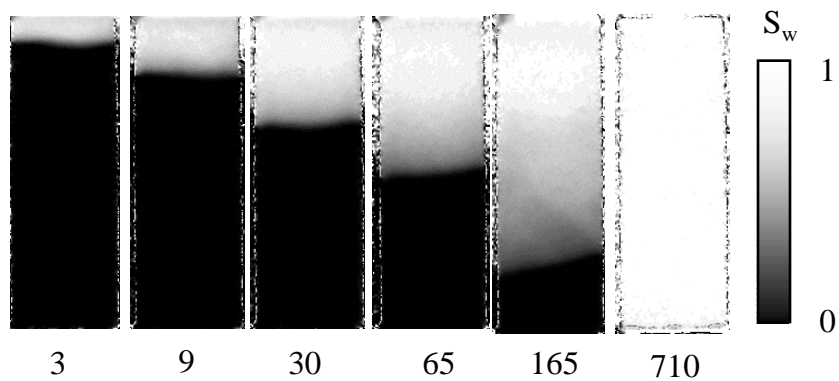


Figure 4. CT-derived water saturation images of counter current water/air imbibition in diatomite. Time is given in minutes beneath the images.

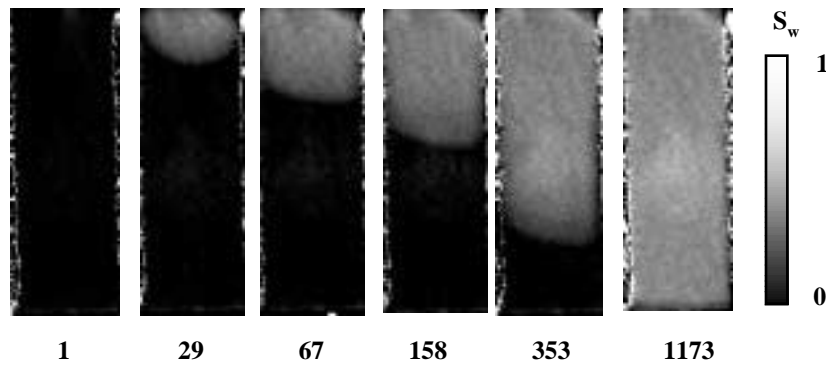


Figure 5. CT-derived water saturation images of counter current water/n-decane imbibition in diatomite. Time is given in minutes given beneath the images.

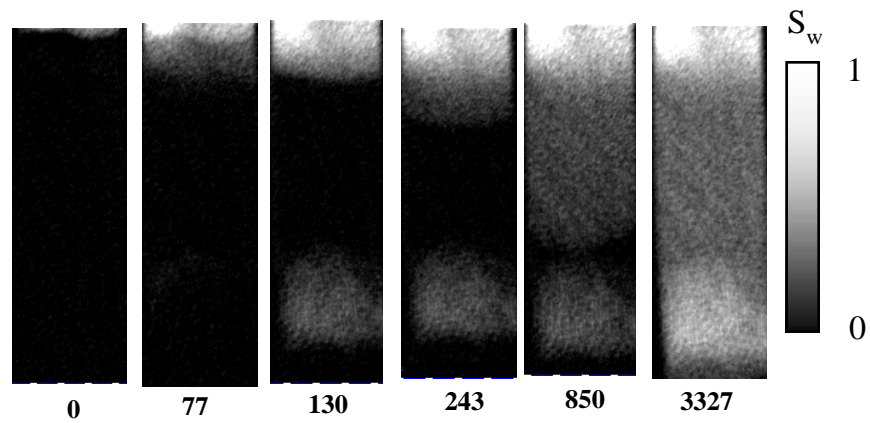
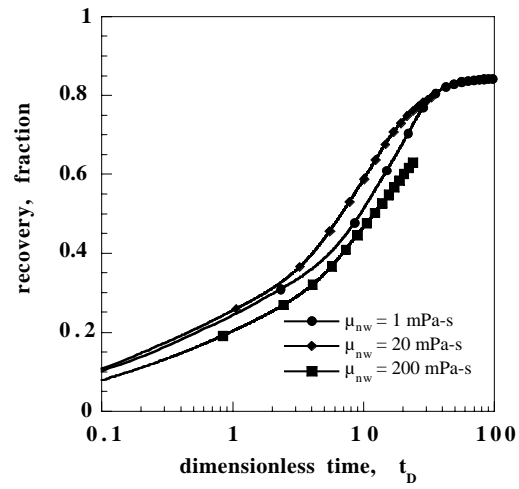
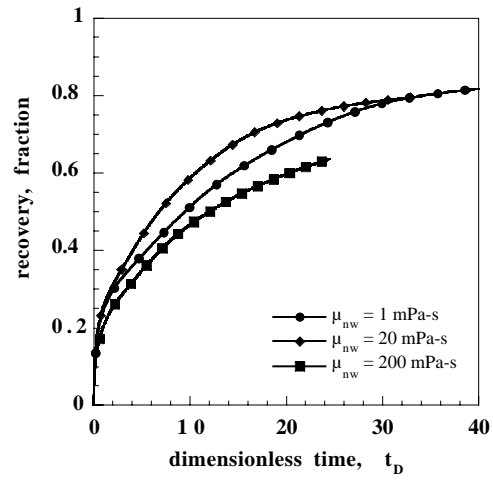


Figure 6. CT-derived water saturation images of counter current water/blandol imbibition in diatomite. Time is given in minutes beneath the images.



(a)



(b)

Figure 7. Scaling of the simulated oil recovery using the dimensionless time of Zhang *et al.* (1996): (a) logarithmic and (b) linear axes for time.

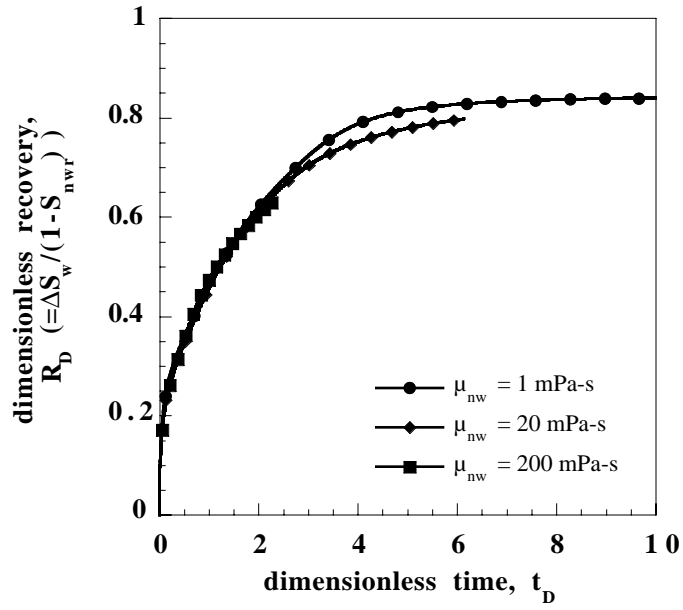


Fig. 8: Scaling of the simulated oil recovery using the proposed dimensionless time.

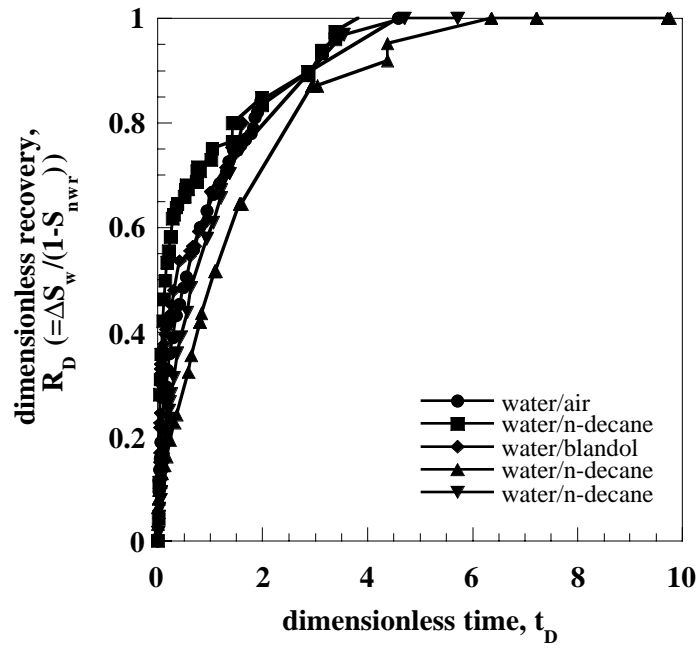


Figure 9. Correlation of recovery by countercurrent imbibition from diatomite using the proposed dimensionless time. Nonwetting-phase viscosity varies by 4 orders of magnitude.